Interaction and dynamics of (alkylamide + electrolyte) deep eutectics: Dependence on alkyl chain-length, temperature, and anion identity

Biswajit Guchhait, Suman Das, Snehasis Daschakraborty, and Ranjit Biswas

Citation: The Journal of Chemical Physics **140**, 104514 (2014); doi: 10.1063/1.4866178
View online: http://dx.doi.org/10.1063/1.4866178
View Table of Contents: http://scitation.aip.org/content/aip/journal/jcp/140/10?ver=pdfcov
Published by the AIP Publishing

Interaction and dynamics of (alkylamide + electrolyte) deep eutectics: Dependence on alkyl chain-length, temperature, and anion identity

Biswajit Guchhait, Suman Das, Snehasis Daschakraborty, and Ranjit Biswas[a)]
Department of Chemical, Biological and Macromolecular Sciences, S. N. Bose National Centre for Basic Sciences, Block-JD, Sector-III, Salt Lake, Kolkata 700098, India

(Received 2 December 2013; accepted 6 February 2014; published online 13 March 2014)

Here we investigate the solute-medium interaction and solute-centered dynamics in ($RCONH_2$ + LiX) deep eutectics (DEs) via carrying out time-resolved fluorescence measurements and all-atom molecular dynamics simulations at various temperatures. Alkylamides ($RCONH_2$) considered are acetamide (CH_3CONH_2), propionamide ($CH_3CH_2CONH_2$), and butyramide ($CH_3CH_2CH_2CONH_2$); the electrolytes (LiX) are lithium perchlorate ($LiClO_4$), lithium bromide (LiBr), and lithium nitrate ($LiNO_3$). Differential scanning calorimetric measurements reveal glass transition temperatures (T_g) of these DEs are ∼195 K and show a very weak dependence on alkyl chain-length and electrolyte identity. Time-resolved and steady state fluorescence measurements with these DEs have been carried out at six-to-nine different temperatures that are ∼100–150 K above their individual T_gs. Four different solute probes providing a good spread of fluorescence lifetimes have been employed in steady state measurements, revealing strong excitation wavelength dependence of probe fluorescence emission peak frequencies. Extent of this dependence, which shows sensitivity to anion identity, has been found to increase with increase of amide chain-length and decrease of probe lifetime. Time-resolved measurements reveal strong fractional power dependence of average rates for solute solvation and rotation with fraction power being relatively smaller (stronger viscosity decoupling) for DEs containing longer amide and larger (weaker decoupling) for DEs containing perchlorate anion. Representative all-atom molecular dynamics simulations of (CH_3CONH_2 + LiX) DEs at different temperatures reveal strongly stretched exponential relaxation of wavevector dependent acetamide self dynamic structure factor with time constants dependent both on ion identity and temperature, providing justification for explaining the fluorescence results in terms of temporal heterogeneity and amide clustering in these multi-component melts. © *2014 AIP Publishing LLC*. [http://dx.doi.org/10.1063/1.4866178]

I. INTRODUCTION

The eternal quest for commercially viable and eco-friendly reaction media has led to the development of several fascinating solvents such as room temperature ionic liquids (RTILs),[1,2] room temperature supercritical fluids (RTSFs),[3,4] and gas expanded liquids (GXLs).[5,6] Deep eutectics (DEs) are mixtures of ionic and non-ionic solid compounds with melting temperature (M_p) much lower than the pure compounds and provide another set of exotic reaction media which exhibit close resemblance to RTILs in solubility and wide liquidous range.[5–13] By carefully choosing components one can introduce in these melts similar longer-ranged interactions (proportional to r^{-1}, r^{-2}, and r^{-3}) to those in dipolar RTILs (RTILs containing dipolar cation and/or anion)[14–19] and moisture stability. Such flexibility provides a boost to construct designer solvents for carrying out chemical reactions with specific and targeted yield. This in conjunction with the ease at which DEs can be prepared at a cost much cheaper than the well-studied imidazolium ILs has rendered these multi-component melts as sustainable alternatives for chemical industry.[9–13] DEs made of alkylamide ($RCONH_2$, R=CH_3, CH_3CH_2, $CH_3CH_2CH_2$) and lithium perchlorate ($LiClO_4$), lithium nitrate ($LiNO_3$) and lithium bromide (LiBr) constitute the subject of the present study where we focus on exploring solute-medium interaction and dynamics via fluorescence measurements and representative computer simulations. The relevance to chemical reaction emerges from the strong and well-established relationship between solvent control and reaction rate.[20,21] Solvent control of a chemical reaction arises from medium polarity and dynamics. Interestingly, these solution aspects of DEs have remained largely unexplored even though these multi-component mixtures possess potential for large scale applications in a variety of sectors ranging from catalytic reactions[12(b)] to metal extraction.[13(b)]

The melting temperatures (M_p) of acetamide (CH_3CONH_2), propionamide ($CH_3CH_2CONH_2$), and butyramide ($CH_3CH_2CH_2CONH_2$) are, respectively, 353 K, 354 K, and 388 K, whereas that of $LiClO_4$ is 509 K.[22,23] However, mixing of these amides with $LiClO_4$ at 81:19 mole ratio produces a colourless liquid at a temperature below 298 K. Likewise, LiBr and $LiNO_3$ are electrolytes with M_p > 500 K but upon mixing with acetamide on certain proportions produces colourless liquids near 300 K. Since these mixtures form liquid solutions at temperatures much below the M_p of individual components, they are sometime also termed as "supercooled" mixtures.[7,8,24–26] Micro-heterogeneity in solution structure may also arise in these (alkylamide + electrolyte) DEs as hydrophobic interaction

a)Author to whom correspondence should be addressed. Electronic mail: ranjit@bose.res.in. Telephone: +91 33 2335 5706. Fax: +91 33 2335 3477.

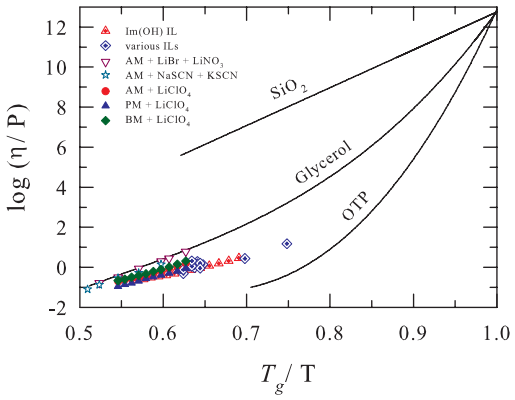

FIG. 1. Viscosity versus reduced inverse temperature plots for various (amide + electrolyte) DEs. Data for three liquid SiO_2, glycerol, and o-terphenyl (OTP) taken from Ref. 28. Data for ILs are taken from Ref. 52.

among alkyl groups and electrostatic interaction between the polar amide group and ions can generate microscopic phase-segregation, leading to formation of microscopic polar and nonpolar domains.[24–26] A competition between the lifetime of these domains and the timescale of a reaction occurring in such media then dictates the heterogeneity-induced modulation of a reaction rate. Moreover, different rates of motions of the environmental particles (that is, temporal heterogeneity)[27–32] can modify a reaction through dynamic solvent effects.[20,33] Consequently, understanding the heterogeneity aspects of these media is critical from basic scientific point of view.

Our earlier studies of molten (acetamide + sodium/potassium thiocyanate)[34] and (acetamide + lithium nitrate/bromide)[35] have revealed strong fractional viscosity dependence of solute solvation and rotation rates, and decoupling between rotation and translation akin to those observed in neat supercooled liquids near glass transition.[27] This observation is in sharp contrast with the results for RTILs where the measured solvation and rotation rates nearly follow the hydrodynamics[36–38] although these RTILs are known to possess high degree of both spatial[39–45] and temporal[46–49] heterogeneities. Recent measurements of solute-centered dynamics in a few RTILs containing alkylated anions also report considerable variation of relaxation rates upon increasing the anionic alkyl chain length.[50] In Fig. 1 we explore the temperature dependence of viscosity of (amide + electrolyte) DE melts studied by us and compare with those for silicon dioxide (SiO_2), glycerol, and ortho-terphenyl (OTP).[28,51] Data for several protic and aprotic imidazolium ILs[52] are also presented in the same figure. Note the types of longer ranged electrostatic interactions (for example, ion-ion, dipole-dipole, and ion-dipole interactions) present in these DEs also govern the statics and dynamics of dipolar RTILs.[16–19] As evidenced by the non-Arrhenius temperature dependence of viscosity, these DEs belong to "fragile" class of liquids and bear a strong resemblance to RTILs in this respect. Note a small difference appears in this temperature dependence of viscosity for these DEs when the perchlorate (ClO_4^-) is replaced by nitrate (NO_3^-), bromide (Br^-), or thiocyanate (SCN^-).

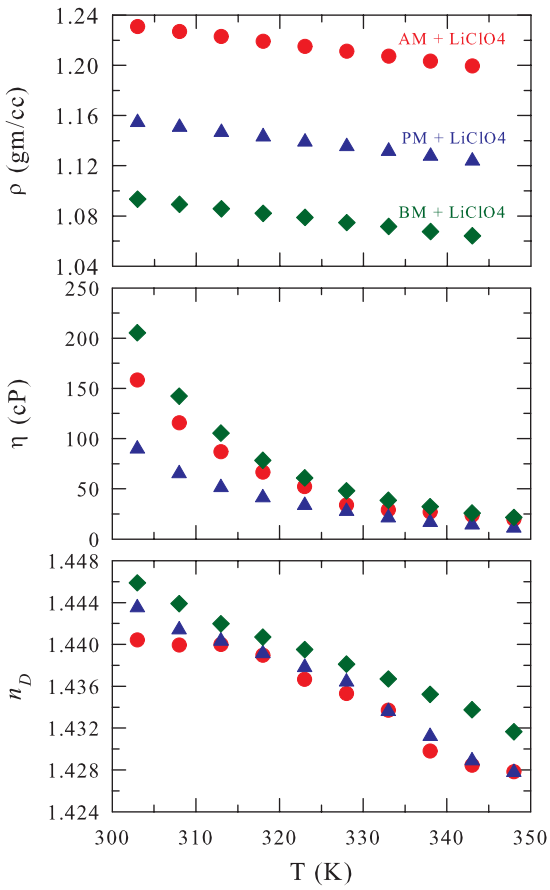

FIG. 2. Experimental density (upper panel), viscosity (middle panel), and refractive index (lower panel) as a function of temperature for the (RCONH2 + LiX) DEs considered here.

The above features and the debate regarding the structure-breaking ability[53–62] of ClO_4^- ion in aqueous media have motivated us to explore the anion dependence of interaction and dynamics in these (amide + electrolyte) DEs. The latter aspect emerges from the H-bonding ability of the amides and the subsequent modification of inter-amide H-bond network in presence of the added ions. Additionally, increase of alkyl chain length is known to induce enhanced spatial heterogeneity in RTILs[40] but a systematic study of such an effect in DEs has not yet been explored. We mentioned here that the construction of DEs containing $RCONH_2$ and $LiClO_4$ at 0.81:0.19 mole fractions has been inspired by the existing phase diagram for molten (alkylamide + sodium trifluoroacetate) system.[63] Glass transition temperatures (T_g) for these melt mixtures have been measured (details in Sec. II) and they are ~195 K (see Fig. S1 of the supplementary material)[64] and do not depend on the alkyl chain length attached to the amide employed. Note this value of T_g and its sensitivity to alkyl chain length are very similar to what have already been observed for a number of RTILs.[52] Temperature dependent densities (ρ), viscosity coefficients (η), and refractive indices (n_D) have also been measured for these ($RCONH_2$ + $LiClO_4$) DEs for better characterization and reported in Fig. 2 and Table S2 of the supplementary material.[64] For variation of the temperature between 303 K and 343 K, ρ and η cover ranges for these DEs spanned by imidazolium cation

based RTILs[18,55] for the similar temperature range. The refractive indices (n_D) for these DES at ~300 K are somewhat larger compared to those for these RTILs[52] at this temperature. A point to note here is that the alkyl chain length dependence of n_D follows a trend reverse to that found for ρ and originates from larger size and electronic polarizability of the amide with longer alkyl chain. Finally, representative molecular dynamics simulations of (CH_3CONH_2 + LiX) DEs with X = ClO_4^-, NO_3^-, and Br^- at various temperatures have been carried out in order to provide microscopic explanations to the observed fluorescence results.

II. EXPERIMENTAL DETAILS

(i) Materials and method: C153 (laser grade, Exciton), 6-propionyl-2-(*N*,*N*- dimethylamino)naphthalene (PRODAN, Fluka), 8-anilino-1-naphthalenesulfonic acid (ANS, Sigma-Aldrich) were used as received. Trans-2-[4-dimethylamino)styryl]benzothiazole (DMASBT) was used without further purification.[35] Acetamide (≥99%, Sigma-Aldrich), propionamide (>97% Sigma-Aldrich), butyramide (98% Merck, Germany), and lithium perchlorate (≥99%, Fluka) were vacuum-dried (at ~300 K) for 48 h before use.

(ii) Sample preparation: The details of sample preparation for spectroscopic investigation of (acetamide + electrolyte) are available in our previous works.[34,35] The concentration of a given fluorophore in each of the samples, taken in an optically transparent quartz cuvette (1 cm path length), was maintained at $\leq 10^{-5}$ M. A temperature controller (Julabo, model-F32) was used for temperature equilibration (better than ±0.5 K). A few samples were bubbled with dry N_2 gas before data collection but did not produce any difference in data with those collected with the un-bubbled samples.

(iii) Density and viscosity measurements: Temperature dependent densities (ρ) of ($RCONH_2$ + $LiClO_4$) DEs were measured by using automated temperature-controlled density-cum-sound analyzer (Anton Paar, model DSA 5000). Subsequently, viscosity coefficients (η) and refractive indices (n_D) were measured by using an automated, temperature-controlled micro viscometer (AMVn, Anton Paar) and refractometer (RUDOLPH, J357), respectively.

(iv) Measurements of glass transition temperature: T_g of the DEs were measured employing the differential scanning calorimetry (DSC, TA Instruments Q2000) technique. The temperature and heat flow were calibrated using a certified indium sample. Measurements were performed in the range of 103–423 K under a flow of 50 ml/min dry N_2 and 25 ml/min He. The samples were hermetically sealed in an aluminium pan (40 μl, Tzero, TA Instruments) to prevent evaporation during the measurements. A heating/cooling rate of 10 K/min and 2 min isothermal periods at 103 K were used for all measurements.

(v) Steady state spectroscopic measurements: Steady-state absorption and emission spectra were collected using a UV-visible spectrophotometer (UV-2450, Shimadzu) and a fluorimeter (Fluoromax-3, Jobin-Yvon, Horiba), respectively. Precautionary measures were taken to avoid moisture absorption by samples during measurements. Solvent blanks were subtracted prior to analysis. All samples were excited at their respective absorption maxima for steady state fluorescence measurements.

(vi) Time-resolved spectroscopic measurements: Time-resolved fluorescence measurements were performed using a time correlated single photon counting (LifeSpec-ps, Edinburgh Instruments, U. K.) set-up.[34,35] The instrument response function (IRF) measured using a diode laser emitting an excitation light with wavelength of 409 nm and water was found to be ~75 ps. We used 409 nm excitation for C153, ANS, DMASBT, and 375 nm for PRODAN. Time-resolved emission spectra (TRES) were synthesized from the collected ~20 intensity decays for each of the samples by following the method discussed in detail elsewhere.[34,35] Solvation response function was then constructed as follows:[65] $S(t) = \{\nu(t) - \nu(\infty)\}/\{\nu(0) - \nu(\infty)\}$, $\nu(x)$ representing the fluorescence frequency at time t, 0, and ∞, respectively. We used first moments of the TRES to determine $S(t)$. Subsequently, the average solvation times were obtained via time-integrating the measured $S(t)$ (found to be bi-exponential) decays:[34,35] $\langle\tau_s\rangle = \int_0^\infty dt\, S(t) = \int_0^\infty dt \sum_{i=1}^2 a_i \exp(-t/\tau_i) = (a_1\tau_1 + a_2\tau_2)$ with $(a_1 + a_2) = 1$.

Time-resolved fluorescence anisotropy ($r(t)$) measurements were done following the standard protocol[34,35] and using the iterative reconvolution for simultaneous fitting of the parallel $\{I_{para}(t)\}$ and the perpendicular $\{I_{perp}(t)\}$ decays.[66–68] The geometric factor (G) was obtained by tail matching the collected $I_{para}(t)$ and $I_{perp}(t)$ decays at time longer than the anticipated rotation time. Normalized $r(t)$ decays, like the $S(t)$ decays, were also found to be bi-exponentials and average rotation times were obtained as follows: $\langle\tau_r\rangle = \int_0^\infty dt[r(t)/r(0)] = \int_0^\infty dt \sum_{i=1}^2 a_i \exp(-t/\tau_i) = (a_1\tau_1 + a_2\tau_2)$ where $r(0)$, denoting the initial anisotropy, was fixed at 0.376[66] (for all samples studied here), and $(a_1 + a_2) = 1$.

III. SIMULATION DETAILS

All-atom molecular dynamics simulations were carried out with a total of 512 particles for ($0.81CH_3CONH_2$ + $0.19LiClO_4$), ($0.78CH_3CONH_2$ + $0.22LiNO_3$), and ($0.78CH_3CONH_2$ + 0.22LiBr) DEs at 303 K and 350 K by using DL_POLY version 2.20.[69] The number of CH_3CONH_2 and ions have been chosen accordingly. For example, for ($0.78CH_3CONH_2$ + 0.22LiBr) DEs we have employed 400 CH_3CONH_2 molecules and 56 pairs of cation and anion. The potential function used has the following form:

$$U(R) = \sum_{bonds} K_r(r - r_{eq})^2 + \sum_{angles} K_\theta(\theta - \theta_{eq})^2 + \sum_{dihedrals} \frac{V_n}{2}(1 + \cos[\eta\varphi - \gamma]) + \sum_{i<j}^{atoms}\left(\frac{A_{ij}}{R_{ij}^{12}} - \frac{B_{ij}}{R_{ij}^{6}}\right) + \sum_{i<j}^{atoms} \frac{q_i q_j}{4\pi\varepsilon_0 R_{ij}}, \quad (1)$$

where R_{ij} is the distance between i and j atom with partial charges q_i and q_j, respectively. The force field parameters for

the acetamide were taken from the CHARMM force field.[70] The force field parameters for Li^+, ClO_4^-, Br^-, and NO_3^- were taken from the existing literature.[71–73] As done earlier,[73] the force field was constructed by using DL_FIELD.[74] The Coulombic interaction was treated by employing the Ewald summation technique.[75]

The initial configuration of a given DE mixture was built using Packmol[76] with large simulation box-length. Then the system was equilibrated in NPT ensemble for 2 ns to reach the experimental density. Finally, the production run was carried out in NVT ensemble for 10 ns, after a further equilibration for 2 ns in this ensemble. The periodic boundary condition was employed and the equation of motion was integrated with a time step of 2 fs using the velocity Verlet algorithm.[75] Subsequently, the wavevector (k) dependent incoherent scattering function, $F_s^N(k, t) = F_s(k, t) / F_s(k, t = 0)$, was obtained via Fourier transforming the simulated self part of the van Hove correlation function,[77] $G_s(\mathbf{r}, t)$, as follows:

$$F_s(\mathbf{k}, t) = \int d\mathbf{r} \exp[-i\mathbf{k}.\mathbf{r}]G_s(\mathbf{r}, t). \quad (2)$$

IV. RESULTS AND DISCUSSIONS

A. Interaction in ($RCONH_2$ + LiX) DEs: Alkyl chain length and anion dependencies from steady state spectral measurements

Solute-medium interactions in ($RCONH_2$ + LiX) DEs have been probed by steady state absorption and fluorescence measurements. Representative absorption and fluorescence spectra of C153 in ($RCONH_2$ + $LiClO_4$) and the resultant spectral characteristics at different temperatures are presented in Fig. 3. The alkyl chain length dependence of such interactions at 303 K is depicted in the first panel where a small blue-shift (in emission) upon replacing acetamide by butyramide can be detected. This is because of relatively lower density of butyramide (see Fig. 2 and Table S2 of the supplementary material[64]) and thus connected to packing of the solvation shell around the solute.[4,78] Note the absorption and emission frequencies in these DEs are in the same range as observed earlier in (CH_3CONH_2 + LiBr/NO_3) DEs[35] but ~200–400 cm^{-1} blue-shifted compared to those in (CH_3CONH_2 + Na/KSCN) systems.[34] Interestingly, fluorescence emission in the present DEs exhibits red-shift upon increasing temperature even though the medium density decreases with it. Similar effects of temperature on dynamic Stokes shift have been predicted for several imidazolium ILs[18] and explained in terms of enhanced solute-ion interaction due to a decrease of static dielectric constant (ε_0) upon raising temperature.[79] In addition, a more complete environmental equilibration at higher temperature can also partly contribute to the observed red-shift of the spectrum at higher temperature.

Another aspect of steady state fluorescence emission in these highly viscous perchlorate containing DEs ($10 < \eta / cP < 210$) that needs consideration is whether the emission occurs from the fully solvent relaxed state of the excited solute. This can be quantified by following the difference between the dynamic Stokes shift ($\Delta\nu^t = \nu_0 - \nu_\infty$) and steady state Stokes shift relative to a non-polar solvent ($\Delta\Delta\nu = (\nu_{abs} - \nu_{em})_{DE} - (\nu_{abs} - \nu_{em})_{NP} = \Delta\nu_{DE} - \Delta\nu_{NP}$). We find that this difference, $\delta\delta\nu = \Delta\nu^t - \Delta\Delta\nu$, appearing due to sluggish solvent relaxation in comparison to the probe lifetime, is the maximum (~400 cm^{-1}) for the butyramide containing DE melt and the minimum (~200 cm^{-1}) for the acetamide containing one (see Fig. S3 of the supplementary material[64]). In addition, $\delta\delta\nu$ in ClO_4^- containing acetamide DEs (~200–400 cm^{-1}) is smaller than that measured[35] in the corresponding DEs containing NO_3^- or Br^-, reflecting a dependence of sort on ion identity.

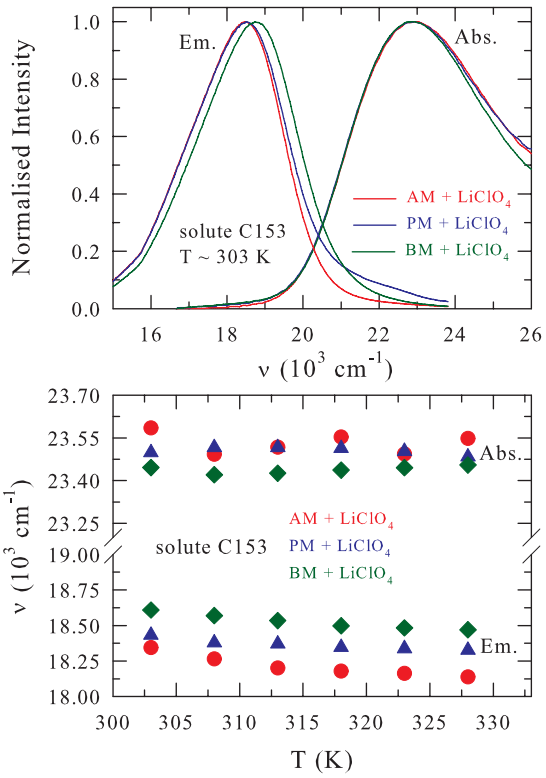

FIG. 3. Steady state absorption and emission spectra of C153 in (alkylamide + $LiClO_4$) DEs (color-coded). The upper panel presents absorption and emission spectra at 303 K. Frequencies (ν_{abs} and ν_{em}) as a function of temperature are shown in the lower panel. Note that acetamide (CH_3CONH_2), propionamide ($CH_3CH_2CONH_2$), and butyramide ($CH_3CH_2CH_2CONH_2$) are represented in this figure by AM, PM, and BM, respectively.

The micro-heterogeneous nature of solution structure is investigated next by using solute probes of differing excited state lifetimes (τ_{life}). τ_{life}($\equiv \tau_{Long}$ of the bi-exponential intensity decay collected) for ANS, C153, PRODAN, and DMASBT in these DEs have been found to be ~6 ns, 4 ns, 3 ns, and 0.5 ns, respectively (see Fig. S4 and Table S5 of the supplementary material[64]). These τ_{life} values are well-correlated with the literature values[35,65,80,81] and thus dynamic quenching effects by ions in the present study can be regarded as negligible. Fig. 4 displays the excitation wavelength ($\lambda_{exc.}$) dependence of fluorescence emission peaks of these solutes. Different $\lambda_{exc.}$ employed for this study are indicated on the respective absorption spectrum in Fig. S6 of the supplementary material.[64] While the upper panel shows the solute dependence of the $\lambda_{exc.}$ induced emission peak shift in (CH_3CONH_2 + $LiClO_4$) at ~303 K, the middle panel displays the alkyl chain length dependence of it with C153 at the same temperature. Results from similar study using

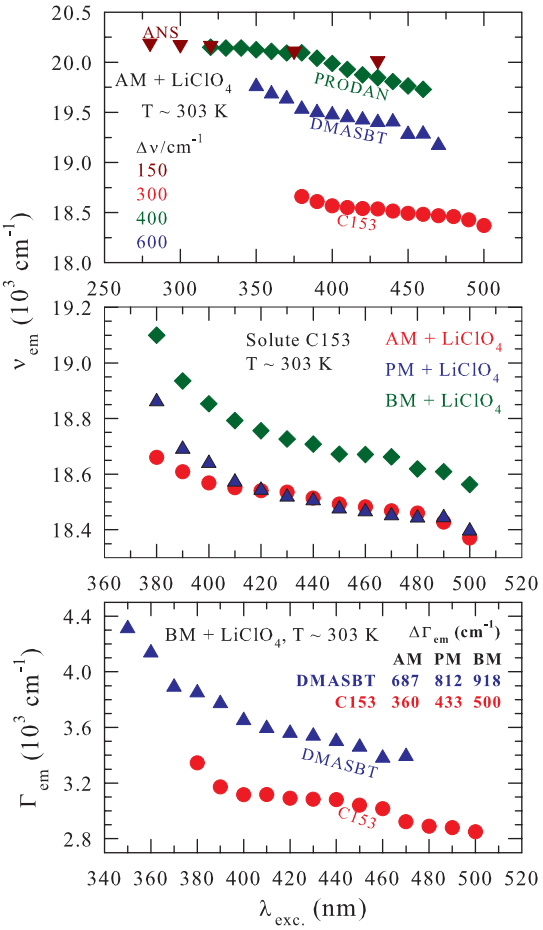

FIG. 4. Excitation wavelength (λ_{exc}) dependence of the emission peak frequency (ν_{em}) for four dipolar solutes, ANS, C153, PRODAN, and DMASBT in (AM + $LiClO_4$) system (upper panel), for C153 in the three (alkylamide + $LiClO_4$) DEs (middle panel) at 303 K, and full-width-of-half-maximum of emission spectra (Γ_{em}) of C153 and DMASBT in butyramide DES at ~303 K (lower panel). The numbers inside the upper panel denote the total shift in the emission peak frequencies of these solutes obtained after exciting at the highest and lowest energies, ($\Delta\nu_{em} = \nu_{em}^{blue} - \nu_{em}^{red}$), at ~303 K. Likewise, the numbers inside the lower panel denote the total amount of emission spectral narrowing at ~303 K, $\Delta\Gamma_{em} = \Gamma_{em}^{blue} - \Gamma_{em}^{red}$, where Γ represents the full-width-at-half-maximum of a given spectrum. Data are, as before, color-coded.

PRODAN and DMASBT are shown in Fig. S7 of the supplementary material.[64] Note the total $\lambda_{exc.}$ dependent emission shift, $\Delta\nu^{em} = \nu^{em}(\lambda_{exc.}^{blue}) - \nu^{em}(\lambda_{exc.}^{red})$, for ($CH_3CONH_2$ + $LiClO_4$) at ~303 K is the largest (~600 cm^{-1}) for DMASBT and the smallest for ANS (~150 cm^{-1}) and thus varies inversely as τ_{life}. This τ_{life} dependence of $\Delta\nu^{em}$ (see also Fig. S8 of the supplementary material[64]) suggests inhomogeneous solvation structure which may have originated from a competition between density relaxation timescale and the stability time for such inhomogeneous solvation structures.[48(a)] Measurements with C153 produces the largest $\Delta\nu^{em}$ (~600 cm^{-1}) for ($CH_3CH_2CH_2CONH_2$ + $LiClO_4$) and the smallest (~300 cm^{-1}) for (CH_3CONH_2 + $LiClO_4$), suggesting more pronounced micro-heterogeneous solution structure for DEs containing amide with longer alkyl chain. This is further supported by the $\lambda_{exc.}$ dependence of the emission spectral width, Γ_{em} (full-width-at-half-maximum, FWHM), shown in the lower panel of Fig. 4. Clearly, moving $\lambda_{exc.}$ to lower energy (higher wavelength) induces substantial narrowing of the emission spectral width of both DMASBT and C153. This is rather a general result for the DEs considered here, reflected via the summary of the total amount of narrowing ($\Delta\Gamma_{em}$) for these solutes shown in the inset. Note $\Delta\Gamma_{em}$ increases as the alkyl chain length increases, indicating more heterogeneous distribution of solvation structures for DEs with longer alkyl chain. Similar effects of alkyl chain have also been observed in studies with RTILs.[40,82]

TABLE I. Anion dependence of $\lambda_{exc.}$ induced total emission shift for a short lifetime probe (DMASBT) and a long lifetime probe (C153) in (CH_3CONH_2 + LiX) DEs at ~303 K.

		$\Delta\nu^{em}$ (cm^{-1})	
Anion	Radius (Å)	DMASBT	C153
ClO_4^-	2.4	600	300
NO_3^-	1.96	1300	300
Br^-	1.82	800	600

The anion dependence of $\Delta\nu^{em}$ obtained by using DMASBT (τ_{life}~ 0.5 ns) and C153 (τ_{life} ~ 4 ns) is shown in Table I where representative results for (CH_3CONH_2 + LiX) DEs at 303 K are presented along with the radii[35,83] of the ions considered. Note the extent of anion dependence of $\Delta\nu^{em}$ is larger for low lifetime probe. Moreover, $\Delta\nu^{em}$ neither shows any correlation with ion size nor follows the Hofmeister sequence of solubility found for electrolytes in non-aqueous media.[84] It is interesting to note that $\Delta\nu^{em}$ found with DMASBT in presence of NO_3^- is twice as large as that in presence of ClO_4^-, while no such anion effects have been observed with C153. This suggests that there might be some ion specific effects on density relaxation timescale and cluster stability, and different geometrical shapes of these anions (NO_3^- being trigonal planar and ClO_4^- tetrahedral)[85] could be one of the factors. However, one needs further study to confirm the specific ion effects on medium density relaxation and the subsequent impact on $\lambda_{exc.}$ induced $\Delta\nu^{em}$.

B. Dynamics in ($RCONH_2$ + LiX) DEs: Dependence on alkyl chain length and anion from time-resolved fluorescence measurements

Next we explore the alkyl chain length and anion dependencies of solute solvation and rotation dynamics in these (amide + electrolyte) DEs by carrying out temperature dependent measurements using C153 as a probe. Typical decay characteristics at blue and red ends, and time-resolved emission spectra for a representative DE are provided in upper and middle panels of Fig. 5 which suggest presence of dynamics spanning picosecond to nanosecond timescales. The widths of these emission spectra, $\Gamma(t)$, shown in the lower panel of the figure, show transient broadening followed by overall narrowing as solvation progresses, which has also been observed earlier for a wide variety of systems that include conventional dipolar solvents,[65] supercooled liquids,[85] other (amide + electrolyte) deep eutectics,[34,35] confined aqueous environments,[86] and explained in terms of inhomogeneous

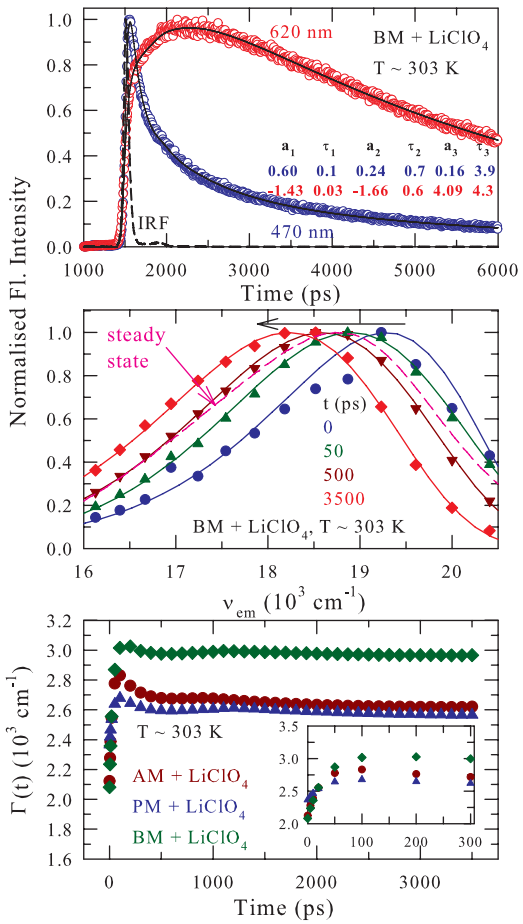

FIG. 5. Representative time-resolved spectral features obtained with C153 in (alkylamide + $LiClO_4$) DEs at ~303 K. While the intensity decay profiles collected at red (620 nm) and blue (470 nm) wavelengths are shown as a function of time in the upper panel, the constructed time resolved emission spectra at different time slices are depicted in the middle one. The lower panel describes the variation of the spectral width (full-width-at-half-maximum) of the time-resolved emission spectrum. The lines going through the collected intensity data (upper panel) are fits and the fit parameters are provided in the inset. Note the fitted time constants (τ_i) are in the unit of nanosecond. The lines joining the geometrical symbols (circles, triangles, etc.) in the middle panel represent log-normal fits to these symbols and depict spectral evolution with time. The inset of the lower panel is for clearer depiction of the dynamic width, $\Gamma(t)$, at the initial stage of the solvent relaxation. All representations are color-coded.

distribution of solvent configurations. Recent dynamic Stokes shift measurements of C153 in RTILs of comparable viscosity have, however, reported monotonic decrease of $\Gamma(t)$ and attributed the observation to the vibrational cooling[87] of the excited solute. Both these factors, inhomogeneous solvent distribution and local heating due to vibrational energy relaxation, may therefore be responsible for the observed behaviour of $\Gamma(t)$ for these DEs.

Table II summarizes the alkyl chain length dependence of dynamic Stokes shift where estimated ($\Delta\nu^t_{est}$)[88] and observed ($\Delta\nu^t_{obs}$) shift magnitudes for C153 in ($RCONH_2$ + $LiClO_4$) DEs at two different temperatures are presented along with the percentage detected by our measurements. Data for four other temperatures are provided in Table S9 of the supplementary material.[64] Note the $\Delta\nu^t_{obs}$ values for these DEs are within ~900–1200 cm^{-1} and decrease with increase of

TABLE II. Alkyl chain-length dependence of dynamic Stokes shift magnitude measured using C153 in ($RCONH_2$ + $LiClO_4$) at two different temperatures. The shift values are better than ±200 cm^{-1}.

Amide	$\Delta\nu^t_{est}$ (cm^{-1})	$\Delta\nu^t_{obs}$ (cm^{-1})	% detected
	T ~ 303 K		
CH_3CONH_2	1243	1191	96
$CH_3CH_2CONH_2$	1129	1025	91
$CH_3CH_2CH_2CONH_2$	963	994	103[a]
	T ~ 313 K		
CH_3CONH_2	1181	1106	94
$CH_3CH_2CONH_2$	1043	980	94
$CH_3CH_2CH_2CONH_2$	1003	994	99

[a]Slightly larger $\Delta\nu^t_{obs}$ than $\Delta\nu^t_{est}$ may arise from the approximations involved in estimating the "true" $\nu(t = 0)$ by using the Fee-Maroncelli method described in Ref. 88. Dynamic Stokes shift measurements using C153 in a few phosphonium ionic liquids reported in Ref. 37 have also indicated similar results, suggesting complete detection of the dynamics.

the alkyl chain length attached to the amide. This may be linked to the decrease of ε_0 with the increase of alkyl chain length.[79] The measured shifts show a weak temperature dependence, suggesting a weak temperature dependence of polarity of the medium surrounding the dissolved solute. Note $\Delta\nu^t_{obs} \approx \Delta\nu^t_{est}$, indicating nearly full detection of the dynamic shifts at these temperatures for these ($RCONH_2$ + $LiClO_4$) DEs by our measurements.

Table III highlights the anion dependence of the dynamic shift measured with C153 in (CH_3CONH_2 + LiX) DEs at two representative temperatures. The observed shift ($\Delta\nu^t_{obs}$) values follow the trend $ClO_4^- > NO_3^- > Br^-$ with the missing component being the largest for (CH_3CONH_2 + LiBr) DEs. Since we used the same temporal resolution (~75 ps) in all measurements, the nearly full detection of dynamic shift for ClO_4^- containing acetamide DEs at these temperatures suggests a specific role for this anion in quenching the ultrafast solvation response by the liquid acetamide molecules in a mixture. In this context it is necessary to recall that amide systems are known to possess collective intermolecular modes centered around ~50–100 cm^{-1} (due to intermolecular H-bonding)[89,90] and these modes, when incorporated in relevant calculations,[91–95] have produced sub-picosecond solvation response. A possible scenario could be that ClO_4^- anion forms complexes with amide in such a way that the amide-amide H-bonding network is substantially disrupted.

TABLE III. Anion dependence of dynamic Stokes shift magnitude measured using C153 in (CH_3CONH_2 + LiX) DEs at two different temperatures. The shift values are better than ±200 cm^{-1}.

Anion	$\Delta\nu^t_{est}$ (cm^{-1})	$\Delta\nu^t_{obs}$ (cm^{-1})	% detected
	T ~ 303 K		
ClO_4^-	1243	1191	96
NO_3^-	1439	993	69
Br^-	1015	650	64
	T ~ 313 K		
ClO_4^-	1181	1106	94
NO_3^-	1409	956	68
Br^-	1265	844	67

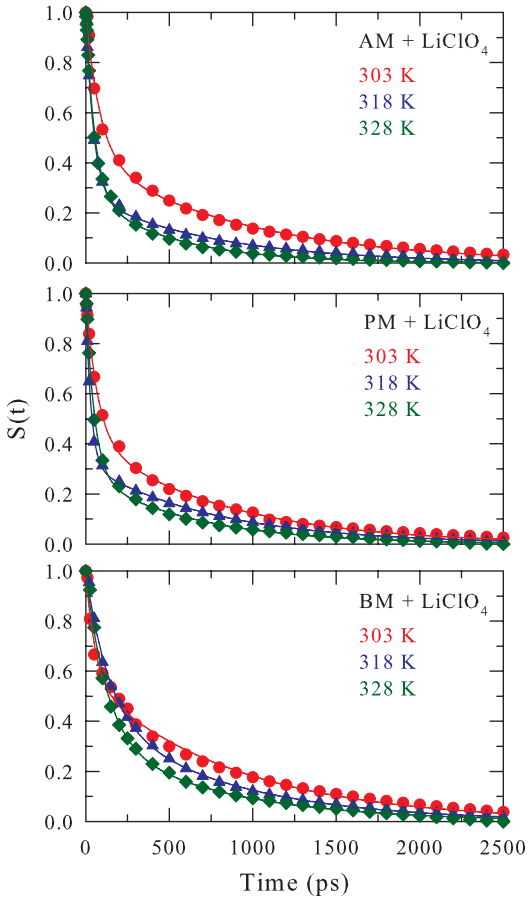

FIG. 6. Temperature dependence of the solvation response function, $S(t)$, measured by using C153 in these DEs. Lines going through the symbols represent bi-exponential fits. Circles represent experimental data at ~303 K, triangles at ~318 K, and squares at 328 K. Representations are also color-coded for visual aid.

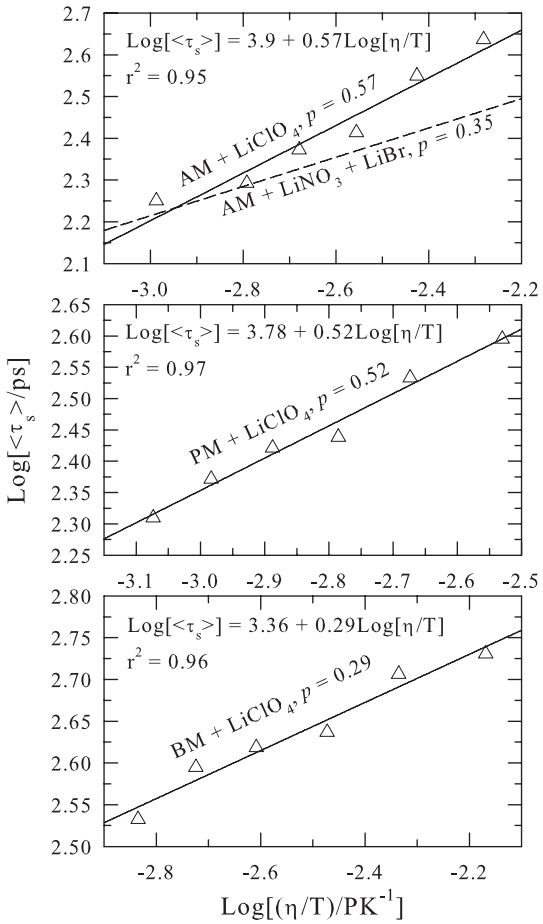

FIG. 7. Log-log plot of average solvation time, $\langle\tau_s\rangle$ versus η/T for C153 in (alkylamide + LiX) DEs showing dependencies on anion and alkyl chain length. Solid lines denote the best linear fits of the measured data to the relation, $Log[\langle\tau_s\rangle/ps] = B + pLog[(\eta/T)/P/K]$. B and p values obtained from fits are also indicated in the respective panels. Dashed lines represent the correlation line obtained via fit of the measured $\langle\tau_s\rangle$ with C153 in (CH_3CONH_2 + LiBr/NO_3) DEs reported in Ref. 35. First panel summarizes the anion dependence of $\langle\tau_s\rangle$ in (CH_3CONH_2 + LiBr/NO_3) DEs.

Interestingly, support for such a view is provided by an existing infrared measurements which reported "no spectral evidence of any residual interamide hydrogen bonds" in mixtures of N-methylpropinamide and $LiClO_4$.[96] Dielectric relaxation measurements with wide frequency coverage and tera-hertz measurements should be carried out to check whether the high frequency absorption is significantly quenched in amide DEs in presence of ClO_4^- but reappears if NO_3^- or Br^- replaces it.

Representative decays of measured solvation response functions with C153 and their bi-exponential fits for ClO_4^- containing amides are provided in Fig. 6 and Table S10 of the supplementary material.[64] The same for Br^- and NO_3^- containing DEs are discussed in our earlier works.[35] As expected, the decay profiles follow, on an average, the medium viscosity and its temperature dependence. Bi-exponential fits to these decays and to those obtained at other temperatures produce a faster component (~50%–75%) with timescale (τ_1) in the ~50–100 ps range, followed by a much slower component with time constant (τ_2) spread over ~0.5–1 ns (see Table S10 of the supplementary material[64]). Interestingly, $\langle\tau_s\rangle$ obtained for these DEs are ~2–4 times faster than those measured recently with the same solute in RTILs of comparable viscosity,[87] reflecting a qualitative difference between these two kinds of media. Fig. 7 summarizes the solute-medium coupling in these media where alkyl chain length and anion dependencies are explored via showing the measured average solvation times ($\langle\tau_s\rangle$) as a function of temperature-reduced viscosity (η/T) in a double logarithmic plot for ($RCONH_2$ + $LiClO_4$) DEs. Fits going through the data points in Fig. 7 indicate fractional viscosity dependence, $\langle\tau_s\rangle = A(\eta/T)^p$, with p significantly smaller than unity ($0.6 > p > 0.3$) in all cases. Note the fraction power (p) in these perchlorate containing amide DEs is the smallest for butyramide (amide with the longest alkyl chain) and the largest for acetamide (amide with the shortest alkyl chain), producing a sequence, $CH_3CH_2CH_2CONH_2 < CH_3CH_2CONH_2 < CH_3CONH_2$. A smaller p value suggests stronger decoupling from medium viscosity and is understood in terms of more pronounced temporal heterogeneity.[27–32] Note this result from time-resolved measurements corroborates well with the steady state fluorescence results presented in Fig. 4 which indicated spatial heterogeneity being the strongest for deep eutectics containing $CH_3CH_2CH_2CONH_2$. This result is also qualitatively similar with observations in dielectric relaxation measurements of RTILs where stronger heterogeneity (reflected by larger value

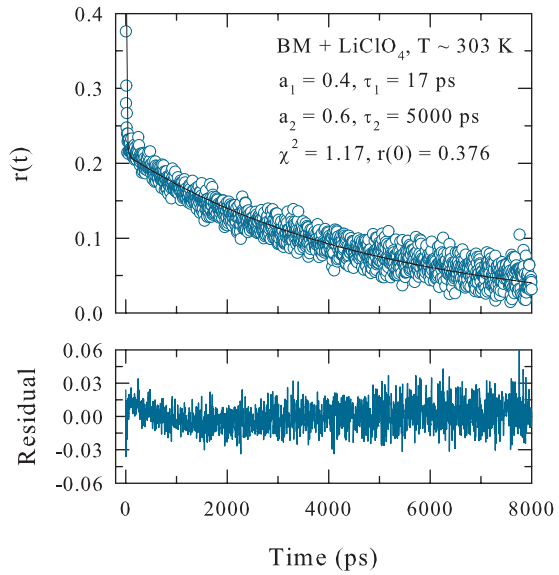

FIG. 8. Dynamic fluorescence anisotropy, $r(t)$, of C153 in (BM + $LiClO_4$) DEs (upper panel) at 303 K and the corresponding residuals (lower panel) of the bi-exponential fit. Fit parameters are also shown in the upper panel. This is a representative figure and fits of similar quality have been obtained for other DEs and temperatures considered in this study.

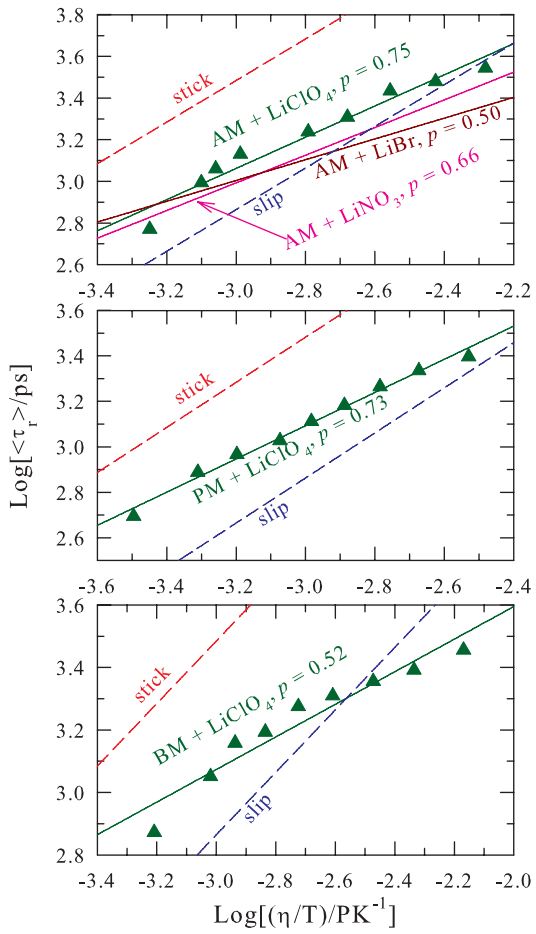

FIG. 9. Log-log plot of average rotation time, $\langle\tau_r\rangle$ versus η/T for C153 in (alkylamide + LiX) DEs, highlighting anion and alkyl chain length dependencies of solute rotation. Solid lines through the data (triangles) in these panels represent the best fits to the relation, $Log[\langle\tau_r\rangle/ps] = B + pLog[(\eta/T)/P/K]$. For AM, PM, and BM the B values are (in proper unit) 5.31, 5.39, and 4.64, respectively. Rotational times obtained from the stick and slip hydrodynamic predictions after incorporating the shape and coupling factors for C153 are also shown. While the first panel summarizes the anion dependence for (CH_3CONH_2 + LiX) DEs, consideration of all the panels reflects the alkyl chain length dependence of $\langle\tau_s\rangle$ in ($RCONH_2$ + $LiClO_4$) DEs.

of α there)[79] has been found for the ionic liquid possessing larger alkyl chain to its dipolar cation.

The anion dependence of p associated with $\langle\tau_s\rangle$ is shown in the first panel of Fig. 7. The $(\eta/T)^p$ dependence for (CH_3CONH_2 + LiBr/NO_3) DEs is presented by the dashed line (p = 0.35).[35] Moreover, separate viscosity dependencies for (CH_3CONH_2 + $LiNO_3$) and (CH_3CONH_2 + LiBr) DEs are not shown separately as data obtained for these individual DEs are too few (because of our limited time-resolution) to extract a meaningful dependence. Even with such a limitation, it is evident that ClO_4^- containing acetamide DEs exhibit more homogeneous (relatively less decoupled as p = 0.57) dynamics than in presence of either Br^- or NO_3^-, suggesting an anion dependence of the fraction power. Note earlier measurements of $\langle\tau_s\rangle$ using C153 in (CH_3CONH_2 + Na/KSCN)[34] DEs have revealed similar fractional viscosity dependence but with p = 0.46. All these results therefore suggest that viscosity decoupling of average solvation rate in (acetamide + electrolyte) DEs is indeed tuned by the electrolyte identity, the microscopic reason for which is still unknown and thus warrants in-depth investigation. Simulation study of anion-dependent amide clustering, and their size and lifetime distributions may help in developing molecular level understanding of these fluorescence results.

The solute-medium coupling and its dependence on alkyl chain length and anion identity is further investigated via monitoring solute rotation in these DEs at various temperatures. Dynamic fluorescence anisotropies (r(t)) collected for ($RCONH_2$ + $LiClO_4$) DEs have been found to fit to bi-exponentials. A representative example of measured r(t) is shown in Fig. 8 along with fit parameters. Table S11 of the supplementary material[64] summarizes the r(t) fit parameters for all such dynamic anisotropies measured here. Note that these r(t) decays are remarkably biphasic with one component (~30%–50%) having time constant much shorter than the IRF and the other with more than a nanosecond. This pronounced biphasic character of r(t) appears irrespective of amide and electrolyte identity and thus can be regarded as a generic feature for these DEs. Note both solvation and rotation rates become faster with increasing the temperature or decreasing the viscosity, indicating a medium viscosity dependence of the measured relaxation rates. Fig. 9 presents the alkyl chain length and anion dependence of average C153 rotation times ($\langle\tau_r\rangle$) in these ($RCONH_2$ + LiX) DEs via a double logarithmic plot of $\langle\tau_r\rangle$ versus η/T. Solid line going through the symbols in each of the panels represents fractional viscosity dependence of C153 rotation times in ($RCONH_2$ + $LiClO_4$) DEs, $\langle\tau_r\rangle \propto (\eta/T)^p$, with p being the smallest for $CH_3CH_2CH_2CONH_2$ (p = 0.52) and the largest for CH_3CONH_2 (p = 0.75). Note p value obtained from solute rotation is larger than that obtained from solute solvation for each of the amides studied here. However, these p values follow the same amide trend as found in the

corresponding viscosity dependence of $\langle\tau_s\rangle$. This observation confirms the alkyl chain length dependence of solute-medium dynamic coupling in one hand, and suggests some sort of rotation-translation decoupling on the other. Stick and slip hydrodynamic predictions[34–36] for C153 rotation in ($RCONH_2$ + $LiClO_4$) DEs shown in each of the panels (dashed lines) highlight the deviation from the conventional hydrodynamic behaviour.

The upper panel of Fig. 9 also depicts the anion dependence of solute rotation in (CH_3CONH_2 + LiX) DEs. The fractional viscosity dependencies of C153 rotation times in (CH_3CONH_2 + $LiNO_3$) and (CH_3CONH_2 + LiBr) DEs obtained from our earlier measurements[35] are shown separately by solid lines. Note here that relatively slower timescales associated with C153 rotation allow us to construct separate and meaningful anion-dependent correlations, which was not possible for $\langle\tau_s\rangle$ because of our limited time resolution. Here again the fraction power is the largest (p = 0.75) when ClO_4^- is present in the acetamide DEs but becomes the smallest (p = 0.5) when Br^- replaces ClO_4^-. Use of $LiNO_3$ instead produces a different fraction power (p = 0.66), further supporting the view that identity of the anion does matter in viscosity decoupling of solute dynamics in DEs considered here. These rotation results also support the conclusion derived from solvation studies that (CH_3CONH_2 + $LiClO_4$) is dynamically more homogeneous than the acetamide DEs in presence of either LiBr or $LiNO_3$. This temporal heterogeneity aspect is investigated next by carrying out all-atom molecular dynamics simulations.

C. Temporal heterogeneity and anion dependence of viscosity decoupling: Insight from molecular dynamics simulations at different temperatures

Fig. 10 depicts the anion dependence of acetamide self dynamic structure factor relaxation, where the simulated $F_S^N(k, t)$ at the nearest neighbour (k = 1.33 $Å^{-1}$) and the lowest accessible (k = 0.18 $Å^{-1}$) wavevectors for (CH_3CONH_2 + $LiNO_3$), (CH_3CONH_2 + LiBr), and (CH_3CONH_2 + $LiClO_4$) DEs at 303 K are presented. The nearest neighbour wavevector corresponds to the first peak of the simulated radial distribution function for carbonyl carbon of acetamide molecules. Solid lines through these simulated data represent best fits. Fit parameters and the average decay times for $F_S^N(k, t)$ are summarized in Table S12 of the supplementary material.[64] Note the decay rates at both the wavevectors are different in presence of different anions, reflecting the anion dependence. Importantly, $F_S^N(k, t)$ at the nearest neighbour wavevector exhibits strongly stretched exponential decay in each case, suggesting heterogeneous relaxation dynamics for acetamide in these DEs. These representative simulation results therefore support the view that $(\eta/T)^p$ dependence of measured $\langle\tau_s\rangle$ and $\langle\tau_r\rangle$ for these DEs arises from temporal heterogeneity, and provide a justification for the anion dependence of the fraction power, p. Note also that while $F_S^N(k, t)$ in presence of Br^- at k = 1.33 $Å^{-1}$ depicts stretched exponential decay with a single time constant, the corresponding decays in presence of either NO_3^- or ClO_4^- require a sum of a fast exponential and a slow stretched exponential. Even though the

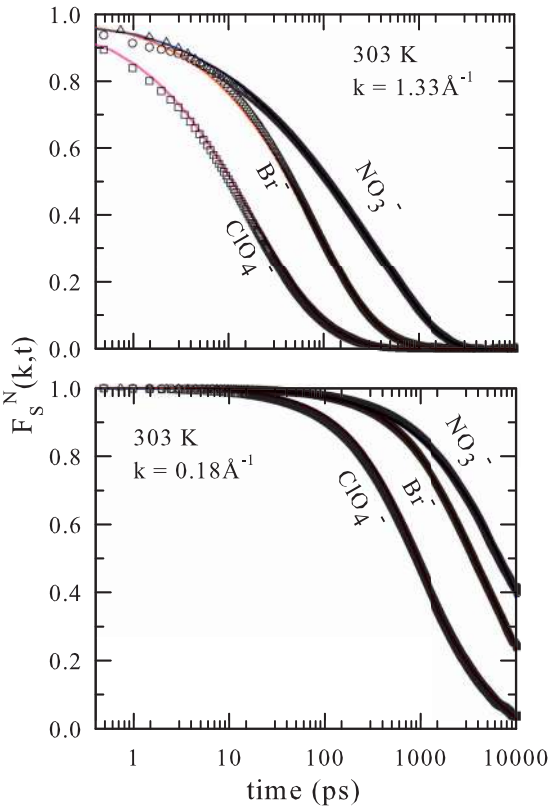

FIG. 10. Anion dependence of acetamide dynamic structure factor relaxation, $F_S^N(k, t)$, simulated for (CH_3CONH_2 + LiX) DEs at 303 K at two wavevectors. While the upper panel presents relaxation at the nearest neighbour wavevector (k = 1.33 $Å^{-1}$), the lower panel shows the data for the lowest accessible wavevector in the present simulations (k ~ 0.18 $Å^{-1}$). Lines going through the simulated data (symbols) are the best fits. Fit parameters are shown in Table S12 of the supplementary material.[64] Note $F_S^N(k, t)$ is a normalized function defined by Eq. (2) in the text.

values for the stretching exponent (β) at k = 1.33 $Å^{-1}$ are not greatly different for these anions, the average relaxation times ($\langle\tau\rangle$) substantially differ. For example, our simulated $\langle\tau\rangle$ is the longest in presence of NO_3^- and the shortest in presence of ClO_4^-. This explains why a fast probe like DMASBT registers the largest $\lambda_{exc.}$ induced emission shift ($\Delta\nu^{em}$, see Table I) for (CH_3CONH_2 + $LiNO_3$) DEs and smallest for (CH_3CONH_2 + $LiClO_4$) DEs. In addition, these average timescales ($\langle\tau\rangle$) also explain why $\Delta\nu^{em}$ is much larger for DMASBT than for C153 as$\langle\tau\rangle$ is related to density relaxation timescales in these media. The $\langle\tau\rangle$ value being much faster in presence of ClO_4^- (~15 and ~3 times faster than those in presence of NO_3^- and Br^-, respectively) also provides a justification for the observed relatively less viscosity decoupling (in other words, larger p values) of solute solvation and rotational dynamics in presence of ClO_4^- than in presence of the other two anions in these (CH_3CONH_2 + LiX) DEs.

$F_S^N(k, t)$ decays at k ~ 0.18 $Å^{-1}$, shown in the lower panel of Fig. 10, describe a much slower relaxation dynamics than those at k = 1.33 $Å^{-1}$ but exhibits the similar anion trend; that is, the decay being the fastest in presence of ClO_4^- and the slowest in presence of NO_3^- with the decay in presence of Br^- in between. The decay rates at both the nearest neighbour and collective wavevectors therefore suggest that dynamics in

presence of ClO_4^- should be the fastest and most homogeneous among the three acetamide DEs studied here. In fact, this has indeed been reflected by our dynamic Stokes shift and anisotropy measurements (Figs. 7 and 9). Interestingly, at both these wavevectors, $F_S^N(k, t)$ relaxation rates in presence of Br^- are faster than those in presence of NO_3^- even though experimental η of (CH_3CONH_2 + LiBr) DEs is larger than that of (CH_3CONH_2 + $LiNO_3$).[35] In addition, the diffusive timescales, σ^2/D, for an acetamide molecule in these DEs calculated from Stokes-Einstein relation with slip boundary condition (using $\sigma_{CH_3CONH_2} = 4.52$ Å, $\eta = 2.11$ P, and 13.12 P, respectively, for NO_3^- containing and Br^- containing DEs at ~303 K)[35] are ~29 ns and ~182 ns. For (CH_3CONH_2 + $LiClO_4$), $\sigma^2/D \approx 20$ ns at the same temperature. These diffusive timescales are evidently much longer than the simulated $\langle\tau\rangle$ values at $k = 0.18$ Å^{-1}. This comparison not only indicates viscosity decoupling of acetamide diffusion in these DEs but also suggests that such decoupling is the most pronounced for (CH_3CONH_2 + LiBr) which is the most viscous among these DEs. These simulation results corroborate well with the anion dependent dynamic Stokes shift and anisotropy measurements for (CH_3CONH_2 + LiX) DEs presented in Figs. 7 and 9.

Subsequently, temperature effects on heterogeneous dynamics of acetamide are explored in Fig. 11 where simulated $F_S^N(k, t)$ corresponding to both the nearest neighbour and collective wavevectors at 303 K and 350 K are compared for (CH_3CONH_2 + LiBr), (CH_3CONH_2 + $LiNO_3$), and (CH_3CONH_2 + $LiClO_4$) DEs. While the best fits through the simulated data points are shown by solid lines, fit parameters and average decay times for $F_S^N(k, t)$ have been summarized in Table S13 of the supplementary material.[64] Clearly, $F_S^N(k, t)$ exhibits heterogeneous dynamics ($\beta \sim 0.6 - 0.7$) at 350 K which is ~150 K above the measured T_g of these deep eutectics. As expected, the acetamide relaxation becomes faster at higher temperature with collective wavevector $\langle\tau\rangle$ at 350 K becoming ~3 times shorter for Br^- containing and ClO_4^- containing DEs, and ~11 times shorter for NO_3^- containing DEs than those at 303 K. For this temperature change, η reduces by a factor of ~20 for (CH_3CONH_2 + LiBr), ~10 for (CH_3CONH_2 + $LiNO_3$), and ~6 for (CH_3CONH_2 + $LiClO_4$) DEs. This again indicates that among these three anions, Br^- induces the most pronounced viscosity decoupling for acetamide relaxation, providing a further support to the conclusion derived from dynamic anisotropy measurements presented earlier. Interestingly, the average of β values obtained in these simulations ($\langle\beta\rangle \approx 0.7$), when used in the fragility versus non-exponentiality ($m - \beta$) correlation,[97] produces a fragility (m) value that corresponds to a domain in the $m - \beta$ plot populated largely by network liquids and alcohols. This correlates well with observation in Fig. 1 where these DEs have been found to exhibit a $\eta - T$ behaviour similar to glycerol.

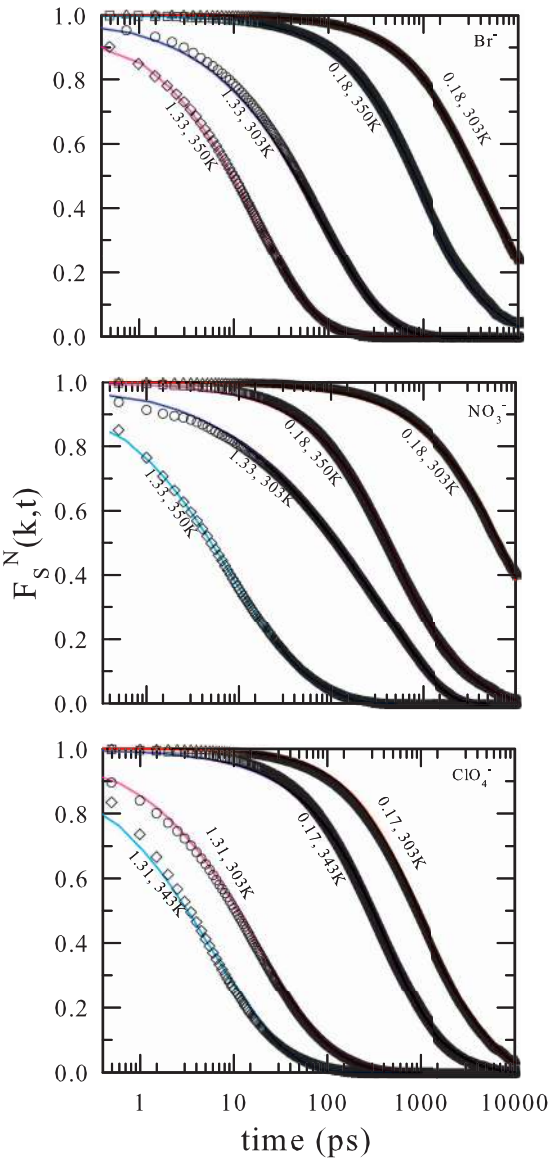

FIG. 11. Temperature dependence of acetamide dynamic structure factor relaxation, $F_s^N(k, t)$ simulated for (CH_3CONH_2 + LiX) DEs at $k = 1.33$ Å^{-1} and $k \sim 0.18$ Å^{-1}. Simulated relaxations are at 303 K and 350 K for these two wavevectors. Results for three different anions are presented in three different panels. Other representations remain the same as in Fig. 10. Fit parameters are shown in Table S13 of the supplementary material.[64]

V. CONCLUDING REMARKS

The main result of the present paper is that the ($RCONH_2$ + LiX) deep eutectics considered here show signatures of both spatial and temporal heterogeneities via exhibiting photo-selection ($\lambda_{exc.}$ dependence), and fractional viscosity dependence of average relaxation rates. The extent of $\lambda_{exc.}$ dependence depends not only on the excited state lifetime of the fluorescent probes but also on the alkyl chain length attached to the amide and the anion identity. While the dependence on probe lifetime may arise from fluctuating solvent environments with dominance of certain timescales, dependence on alkyl chain length and anion identity suggests tuning of inhomogeneous solvent distribution by these system aspects. Fractional viscosity dependence of average rates also exhibits dependence on alkyl chain length and anion identity, indicating dynamic heterogeneity and its tuning by the alkyl chain length and anion. Unlike the viscosity and fluorescence anisotropy, Stokes shift dynamics become slower with longer alkyl chain

(more evident at T ≥ 313 K) which bears qualitative similarity with picoseconds dynamics measured earlier with aqueous amide solutions employing femtosecond Raman-induced Kerr effect spectroscopy.[98]

All-atom simulations reveal stretched exponential relaxation of wavevector dependent amide dynamic structure factors, supporting the explanation of fluorescence results in terms of medium temporal heterogeneity. Simulated dynamic structure factor shows stretched exponential relaxation even at 350 K, revealing existence of heterogeneous amide dynamics in these media at a temperature ∼150 K above T_g. The magnitudes of anion dependent $\lambda_{exc.}$ induced emission shift of a fast probe correlate well with the average relaxation times found for amide dynamic structure factor at the collective wavevector for (CH_3CONH_2 + LiX) deep eutectics. Use of a longer lifetime probe reduces the extent of $\lambda_{exc.}$ induced emission shift, signalling a lifetime distribution of clusters or domains that might have formed in these media via amide-amide and amide-electrolyte interactions. There may also exist amide chain length and anion dependent cluster size and lifetime distributions. Our preliminary simulation data indicate cluster sizes involving five to twelve acetamide molecules in such DEs at ∼300 K which are sensitive to anion identity and which possess different lifetimes. The orientational motion of the acetamide molecules also appear to exhibit jump-like[99] dynamics. It would be interesting to explore how the jump-like dynamics modifies itself in presence of mono and divalent ions in these DEs,[100] and how such a decoupling of dynamics from medium viscosity affects a simple chemical reaction, for example, *cis-trans* isomerisation reaction[101] in these media. Complete measurements of Stokes shift dynamics and dielectric relaxation similar to what has been done for (ionic liquid + polar solvent) binary mixtures,[102, 103] and interpreting them using molecular theories[104–106] and simulations[107] are therefore necessary for a detailed understanding of interaction and dynamics of these complex yet fascinating solvent systems.

ACKNOWLEDGMENTS

S. Das, S. Daschakraborty, and B. Guchhait thank the CSIR, India for providing research fellowships. The work reported here is supported partially by the UNANST project at the Centre and the TUE-CMS project (SR/NM/NS-29/2011(G).

[1] T. Welton, Chem. Rev. **99**, 2071 (1999).
[2] P. Wasserscheid and W. Keim, Angew. Chem. Int. Ed. **39**, 3772 (2000).
[3] R. Noyori, Chem. Rev. **99**, 353 (1999).
[4] J. E. Lewis, R. Biswas, A. G. Robinson, and M. Maroncelli, J. Phys. Chem. B **105**, 3306 (2001).
[5] J. P. Hallett, C. L. Kitchens, R. Hernandez, C. L. Liotta, and C. A. Eckert, Acc. Chem. Res. **39**, 531 (2006).
[6] C. A. Eckert, C. L. Liotta, D. Bush, J. S. Brown, and J. P. Hallett, J. Phys. Chem. B **108**, 18108 (2004).
[7] A. Amico, G. Berchiesi, C. Cametti, and A. D. Biasio, J. Chem. Soc. Faraday Trans. 2 **83**, 619 (1987).
[8] G. Berchiesi, J. Mol. Liq. **83**, 271 (1999).
[9] A. P. Abbott, D. Boothby, G. Capper, D. L. Davies, and R. K. Rasheed, J. Am. Chem. Soc. **126**, 9142 (2004).
[10] A. P. Abbott, G. Capper, D. L. Davies, R. K. Rasheed, and V. Tambyrajah, Chem. Commun. **1**, 70 (2003).
[11] A. P. Abbott, G. Capper, D. L. Davies, H. L. Munro, R. K. Rasheed, and V. Tambyrajah, Chem. Commun. **19**, 2010 (2001).
[12] (a) A. P. Abbott, G. Capper, D. L. Davies, and R. K. Rasheed, Inorg. Chem. **43**, 3447 (2004); (b) A. P. Abbott, G. Capper, D. L. Davies, R. K. Rasheed, and V. Tambyrajah, Green. Chem. **4**, 24 (2002).
[13] (a) A. P. Abbott, G. Capper, D. L. Davies, and R. K. Rasheed, Chem. Eur. J. **10**, 3769 (2004); (b) A. P. Abbott, K. E. Ttaib, G. Frisch, K. J. McKenzie, and K. S. Ryder, Phys. Chem. Chem. Phys. **11**, 4269 (2009).
[14] M. Maroncelli, X.-X. Zhang, M. Liang, D. Roy, and N. P. Ernsting, Faraday Discuss. **154**, 409 (2012).
[15] B. L. Bhargava and S. Balasubramanian, J. Phys. Chem. B **111**, 4477 (2007).
[16] H. K. Kashyap and R. Biswas, J. Phys. Chem. B **112**, 12431 (2008).
[17] H. K. Kashyap and R. Biswas, J. Phys. Chem. B **114**, 254 (2010).
[18] H. K. Kashyap and R. Biswas, J. Phys. Chem. B **114**, 16811 (2010).
[19] S. Daschakraborty and R. Biswas, J. Chem. Phys. **137**, 114501 (2012).
[20] G. van der Zwan and J. T. Hynes, Chem. Phys. **152**, 169 (1991).
[21] T. Pradhan and R. Biswas, J. Phys. Chem. A **111**, 11524 (2007).
[22] J. A. Mitchell and E. E. Reid, J. Am. Chem. Soc. **53**, 1879 (1931).
[23] *CRC Handbook of Chemistry and Physics*, 81st ed., edited by D. R. Lide (CRC Press, Boca Raton, FL, 2007).
[24] M. Gusteri, V. Bartocci, F. Castellani, and F. Pucciarelli, J. Electroanal. Chem. **102**, 199 (1979).
[25] F. Castellani, G. Berchiesi, F. Pucciarelli, and V. Bartocci, J. Chem. Eng. Data **26**, 150 (1981).
[26] G. Berchiesi, M. D. Angelis, G. Rafaiani, and G. Vitali, J. Mol. Liq. **51**, 11 (1992).
[27] M. D. Ediger, Annu. Rev. Phys. Chem. **51**, 99 (2000).
[28] M. D. Ediger, C. A. Angell, and S. R. Nagel, J. Phys. Chem. **100**, 13200 (1996).
[29] H. J. Sillescu, J. Non-Cryst. Solids **243**, 81 (1999).
[30] D. Chakrabarti and B. Bagchi, Phys. Rev. Lett. **96**, 187801(1) (2006).
[31] C. T. Moynihan, J. Phys. Chem. **70**, 3399 (1966).
[32] C. A. Angell, J. Chem. Phys. **46**, 4673 (1967).
[33] K. Dahl, R. Biswas, N. Ito, and M. Maroncelli, J. Phys. Chem. B **109**, 1563 (2005).
[34] B. Guchhait, H. A. R. Gazi, H. K. Kashyap, and R. Biswas, J. Phys. Chem. B **114**, 5066 (2010).
[35] B. Guchhait, S. Daschakraborty, and R. Biswas, J. Chem. Phys. **136**, 174503 (2012).
[36] H. Jin, G. A. Baker, S. Arzhantsev, J. Dong, and M. Maroncelli, J. Phys. Chem. B **111**, 7291 (2007).
[37] N. Ito, S. Arzhantsev, M. Heitz, and M. Maroncelli, J. Phys. Chem. B **108**, 5771 (2004).
[38] A. Samanta, J. Phys. Chem. B **110**, 13704 (2006).
[39] A. Triolo, O. Russina, H. Bleif, and E. D. Cola, J. Phys. Chem. B **111**, 4641 (2007).
[40] A. Triolo, O. Russina, B. Fazio, R. Triolo, and E. D. Cola, Chem. Phys. Lett. **457**, 362 (2008).
[41] A. Triolo, O. Russina, B. Fazio, G. B. Appetecchi, M. Carewska, and S. Passerini, J. Chem. Phys. **130**, 164521 (2009).
[42] P. K. Mandal, M. Sarkar, and A. Samanta, J. Phys. Chem. A **108**, 9048 (2004).
[43] D. K. Sasmal, A. K. Mandal, T. Mondal, and K. Bhattacharyya, J. Phys. Chem. B **115**, 7781 (2011).
[44] H. Jin, X. Li, and M. Maroncelli, J. Phys. Chem. B **111**, 13473 (2007).
[45] A. Adhikari, A. K. Sahu, S. Dey, S. Ghosh, U. Mandal, and K. Bhattacharyya, J. Phys. Chem. B **111**, 12809 (2007).
[46] Y. Wang and G. A. Voth, J. Am. Chem. Soc. **127**, 12192 (2005).
[47] S. S. Sarangi, W. Zhao, F. Muller-Plathe, and S. Balasubramanian, ChemPhysChem **11**, 2001 (2010).
[48] (a) Z. Hu and C. Margulis, J. Proc. Natl. Acad. Sci. U.S.A. **103**, 831 (2006); (b) J. Habasaki and K. L. Nagi, J. Chem. Phys. **129**, 194501 (2008).
[49] T. Pal and R. Biswas, Theo. Chem. Acct. **132**, 1348 (2013).
[50] (a) S. K. Das and M. Sarkar, J. Phys. Chem. B **116**, 194 (2012); (b) S. K. Das and M. Sarkar, ChemPhysChem **13**, 2761 (2012).
[51] I. Chang, F. Fujara, B. Geil, G. Heuberger, T. Mangel, and H. Sillescu, J. Non-Cryst. Solids **172–174**, 248 (1994).
[52] H. Jin, B. O'Hare, S. Arzhantsev, G. Baker, J. F. Wishart, A. J. Binesi, and M. Maroncelli, J. Phys. Chem. **112**, 81 (2008).
[53] G. E. Walrafen, J. Chem. Phys. **52**, 4176 (1970).
[54] G. V. Bondarenko and Y. E. Gorbaty, Mol. Phys. **109**, 783 (2011).
[55] J. Chandrasekhar and W. L. Jorgensen, J. Chem. Phys. **77**, 5080 (1982).

[56]S. Obst and H. Bradaczek, J. Phys. Chem. **100**, 15677 (1996).
[57]A. Tongraar, K. R. Liedl, and B. M. Rode, J. Phys. Chem. **102**, 10340 (1998).
[58]J. Chandrasekhar, D. C. Spellmeier, and W. L. Jorgensen, J. Am. Chem. Soc. **106**, 903 (1984).
[59]S. B. Zhu and G. W. Robinson, J. Chem. Phys. **97**, 4336 (1992).
[60]J. A. White, E. Schwegler, G. Galli, and F. Gygi, J. Chem. Phys. **113**, 4668 (2000).
[61]F. C. Lightstone, E. Schwegler, R. Q. Hood, F. Gygi, and G. Galli, Chem. Phys. Lett. **343**, 549 (2001).
[62]A. W. Omta, M. F. Kropman, S. Woutersen, and H. J. Bakker, Science **301**, 347 (2003).
[63]G. G. Lobbia and G. Berchiesi, Thermochim. Acta **74**, 251 (1984).
[64]See supplementary material at http://dx.doi.org/10.1063/1.4866178 containing DSC scan for determining T_g, figures showing temperature dependence of density, viscosity and refractive index, temperature dependent relative and estimated time-resolved shifts, probe intensity decays and their fit parameters, steady state excitation wavelength dependence of emissions of DMASBT and PRODAN, probe lifetime dependence of $\lambda_{exc.}$ induced emission shifts, time-resolved spectra, temperature dependent dynamic shifts, representative dynamic anisotropy fit, and fit parameters.
[65]M. L. Horng, J. A. Gardecki, A. Papazyan, and M. Maroncelli, J. Phys. Chem. **99**, 17311 (1995).
[66]M. L. Horng, J. A. Gardecki, A. Papazyan, and M. Maroncelli, J. Phys. Chem. A **101**, 1030 (1997).
[67]R. Biswas, A. R. Das, T. Pradhan, D. Touraud, W. Kunz, and S. Mahiuddin, J. Phys. Chem. B **112**, 6620 (2008).
[68]N. Sarma, J. M. Borah, S. Mahiuddin, H. A. R. Gazi, B. Guchhait, and R. Biswas, J. Chem. Phys. B **115**, 9040 (2011).
[69]W. Smith and T. R. Forester, The DL_POLY Molecular Simulation Package, Daresbury Laboratory, Cheshire, U.K., 1999.
[70]A. D. MacKerell, Jr., J. Wiórkiewicz–Kuczera, and M. Karplus, J. Am. Chem. Soc. **117**, 11946 (1995).
[71]K. P. Jensen and W. L. Jorgensen, J. Chem. Theory Comput. **2**, 1499 (2006).
[72](a) C. Cadena and E. J. Maginn, J. Phys. Chem. B **110**, 18026 (2006); (b) G. Papoyan, K. Gu, J. Wiorkiewicz-Kuczera, K. Kuczera, and K. Bowman-James, J. Am. Chem. Soc. **118**, 1354 (1996).
[73]A. Das, S. Das, and R. Biswas, Chem. Phys. Lett. **581**, 47 (2013).
[74]C. W. Yong, DL_FIELD, STFC Daresbury Laboratory, 2011.
[75]M. P. Allen and D. J. Tildesley, *Computer Simulation of Liquids* (Oxford University Press, New York, 1987).
[76]L. Martínez, R. Andrade, E. G. Birgin, and J. M. Martínez, J. Comput. Chem. **30**, 2157 (2009).
[77]J. P. Hansen and I. R. McDonald, *Theory of Simple Liquids*, 3rd ed. (Academic, San Diego, 2006).
[78]R. Biswas, J. E. Lewis, and M. Maroncelli, Chem. Phys. Lett. **310**, 485 (1999).
[79]J. Hunger, A. Stoppa, S. Schrodle, G. Hefter, and R. Buchner, Chem. Phys. Chem. **10**, 723 (2009).
[80]Z. Sun, L. Jin, W. Shi, M. Wei, D. G. Evans, and X. Duan, Langmuir **27**, 7113 (2011).
[81]N. Ito, S. Arzhantsev, and M. Maroncelli, Chem. Phys. Lett. **396**, 83 (2004).
[82]D. C. Khara, J. P. Kumar, N. Mondal, and A. Samanta, J. Phys. Chem. B **117**, 5156 (2013).
[83]*In Supramolecular Chemistry of Anions*, edited by A. Bianchi, K. Bowman-James, and E. Garcia-Espana (Wiley-VCH, NY, 1997), pp. 1–44.
[84]N. Peruzzi, B. W. Ninham, P. L. Nostro, and P. Baglioni, J. Phys. Chem. B **116**, 14398 (2012).
[85]R. Richert and A. Wagener, J. Phys. Chem. **95**, 10115 (1991).
[86]B. Guchhait, R. Biswas, and P. Ghorai, J. Phys. Chem. B **117**, 3345 (2013).
[87]X.-X. Zhang, M. Liang, N. P. Ernsting, and M. Maroncelli, J. Phys. Chem. B **117**, 4291 (2013).
[88]R. S. Fee and M. Maroncelli, Chem. Phys. **183**, 235 (1994).
[89]Y. J. Chang and E. W. Castner, Jr., J. Phys. Chem. **98**, 9712 (1994).
[90]H. Shirota and E. W. Castner, Jr., J. Am. Chem. Soc. **123**, 12877 (2001).
[91]R. Biswas and B. Bagchi, J. Phys. Chem. **100**, 1238 (1996).
[92]H. K. Kashyap, T. Pradhan, and R. Biswas, J. Chem. Phys. **125**, 174506 (2006).
[93]B. Bagchi and R. Biswas, Adv. Chem. Phys. **109**, 207 (1999).
[94]S. Roy and B. Bagchi, J. Chem. Phys. **99**, 9938 (1993).
[95]N. Nandi, S. Roy, and B. Bagchi, J. Chem. Phys. **102**, 1390 (1995).
[96]A. F. Diorio, E. Lippincott, and L. Mandelkern, Nature (London) **195**, 1296 (1962).
[97]R. Böhmer, K. L. Ngai, C. A. Angell, and D. J. Plazek, J. Chem. Phys. **99**, 4201 (1993).
[98]H. Shirota and H. Ushiyama, J. Phys. Chem. B **112**, 13542 (2008).
[99]D. Laage and J. T. Hynes, Science **311**, 832 (2006).
[100]H. A. R. Gazi, B. Guchhait, S. Daschakraborty, and R. Biswas, Chem. Phys. Lett. **501**, 358 (2011).
[101]R. K. Murarka, S. Bhattacharyya, R. Biswas, and B. Bagchi, J. Chem. Phys. **110**, 7365 (1999).
[102]X.-X. Zhang, M. Liang, J. Hunger, R. Buchner, and M. Maroncelli, J. Phys. Chem. B **117**, 15356 (2013).
[103]M. Liang, X.-X. Zhang, A. Kaintz, N. P. Ernsting, and M. Maroncelli, J. Phys. Chem. B **118**, 1340 (2014).
[104]S. Daschakraborty and R. Biswas, J. Phys. Chem. B **115**, 4011 (2011).
[105]S. Daschakraborty and R. Biswas, J. Phys. Chem. B **118**, 1327 (2014).
[106]S. Daschakraborty and R. Biswas, J. Chem. Phys. **140**, 014504 (2014).
[107]T. Pal and R. Biswas, Chem. Phys. Lett. **517**, 180 (2011).